Parameterizations and Algorithms for Oceanic Whitecap Coverage

LONNEKE GODDIJN-MURPHY AND DAVID K. WOOLF

Environmental Research Institute, Thurso, United Kingdom

ADRIAN H. CALLAGHAN*

Department of Earth and Ocean Sciences, National University of Ireland, Galway, Ireland

(Manuscript received 26 July 2010, in final form 16 December 2010)

ABSTRACT

Shipboard measurements of fractional whitecap coverage W and wind speed at 10-m height, obtained during the 2006 Marine Aerosol Production (MAP) campaign, have been combined with ECMWF wave model and Quick Scatterometer (QuikSCAT) satellite wind speed data for assessment of existing W parameterizations. The wind history trend found in an earlier study of the MAP data could be associated with wave development on whitecapping, as previously postulated. Whitecapping was shown to be mainly wind driven; for high wind speeds (>9 m s^{-1}), a minor reduction in the scatter of in situ W data points could be achieved by including sea state conditions or by using parameters related to wave breaking. The W values were slightly larger for decreasing wind/developed waves than for increasing wind/developing waves, whereas cross-swell conditions (deflection angle between wind and swell waves between $\pm 45°$ and $\pm 135°$) appeared to dampen whitecapping. Tabulated curve fitting results of the different parameterizations show that the errors that could not be attributed to the propagation of the standard error in U_{10} remained largely unexplained. It is possible that the counteracting effects of wave development and cross swell undermine the performance of the simple parameterizations in this study.

1. Introduction

Breaking waves generate turbulence and entrain air at the surface, resulting in sea spray and whitecaps (bubbles and foam). Whitecapping has been studied by various authors for a number of reasons. By altering spectral reflectance and roughness of the ocean surface, whitecaps affect satellite remote sensing of ocean color (Gordon 1997) and wind vectors (Quilfen et al. 2007). Breaking waves and whitecaps enhance air–sea gas transfer (Asher et al. 1996; Woolf et al. 2007) and knowledge of the variation of whitecapping can therefore improve the calculation of gas fluxes between ocean and atmosphere (Woolf 2005). For greenhouse gasses such as CO_2, this information is relevant for climate studies. Whitecaps are associated with marine primary aerosol production (sea spray particles), and whitecap coverage has been used to estimate aerosol fluxes over the ocean (Monahan et al. 1986; O'Dowd and de Leeuw 2007). Finally, a better understanding of whitecapping is highly in demand by wave modelers, because whitecaps relate to energy dissipation of waves, the least known process of wave evolution. Whitecaps are presently used as a ''tuning knob'' of any wave model (Cavaleri et al. 2007).

A common quantification of whitecaps is the spatial fraction of whitecap coverage W (unless stated otherwise, the unit for W in this paper is percent). Because whitecaps are mainly wind driven, most W parameterizations are a function of wind speed. Almost all relationships between wind speed and W are described by a power law or by a function of cubed wind speed. Summaries of ''wind speed only'' empirical parameterizations are given by Zhao and Toba (2001) and Anguelova and Webster (2006). The large differences in the listed parameterizations and the scatter within the various datasets imply that additional factors play a role in the whitecap formation. In this study, we compare a selection of published W algorithms, which are based

* Current affiliation: School of Physics and Ryan Institute, National University of Ireland, Galway, Ireland.

Corresponding author address: Dr. Lonneke Goddijn-Murphy, Environmental Research Institute, UHI–North Highland College, Castle Street, Thurso KW14 7NX, United Kingdom.
E-mail: lonneke.goddijn-murphy@thurso.uhi.ac.uk

DOI: 10.1175/2010JPO4533.1

on wind speed and sea state, using an in situ wind speed and W dataset. We combine these field measurements with wind and wave model data of the European Centre for Medium-Range Weather Forecasts (ECMWF) and with wind speed retrievals from the SeaWinds scatterometer on the Quick Scatterometer (QuikSCAT) satellite. In situ data were obtained in the northeast Atlantic during the 2006 Marine Aerosol Production (MAP) survey (Callaghan et al. 2008b). This is an important dataset because of the occurrence of high wind speeds and the detection of an apparent dependence on wind history, among other features. However, sea state was not measured and whitecap coverage was parameterized solely in terms of ship-board wind speed. The data can be divided into two overlapping groups: all W data points measured at wind speeds below 11.25 m s^{-1} and all W data points above 9.25 m s^{-1}. Applying a simple regression of $W^{1/3}$ versus wind speed, it was determined that the regression slope for the lower wind speeds is steeper than the regression slope over the higher wind speeds (Callaghan et al. 2008b, Fig. 1). At wind speeds above 9.25 m s^{-1}, W is generally larger for periods of decreasing wind compared to periods of increasing wind in terms of 2.5-h wind history (Callaghan et al. 2008b, Fig. 2). At wind speeds below 9.25 m s^{-1}, any sensitivity to wind history is not apparent. These results depend on the accuracy of the ship-based wind measurements; therefore, the independent datasets available to this study are useful 1) to check the robustness of results from the original study and 2) because it is always difficult to extrapolate from ship-based wind speeds to the globe, whereas satellite and model values are universally available and their accuracy and homogeneity have been studied previously (e.g., Caires and Sterl 2003, 2005; Quilfen et al. 2007). In this study we address the following objectives:

1) testing the grouping of W data points in higher and lower wind speeds and wind history trend, using model and satellite wind speed data and
2) assessing additional existing W parameterizations based on wind speed and sea state parameters, using universally available data.

2. Existing parameterizations

a. Wind speed only

The most common W parameterizations take the form of a power-law relation between W and U_{10},

$$W = aU_{10}^{b} \tag{1}$$

with coefficients a and b derived from a best fit of a set of observations. The values for a and b vary widely with different locations and conditions. In tabulated overviews of examples in whitecap literature, the exponent b ranges from 2.0 to 5.16, with an average of roughly 3 (Zhao and Toba 2001; Anguelova and Webster 2006).

The term W has also been related to cubed wind speed,

$$W = a(U_{10} + b)^{3} \tag{2}$$

(e.g., Anguelova and Webster 2006; Sugihara et al. 2007; Callaghan et al. 2008b). Regarding the in situ data, linear regression between $W^{1/3}$ and U_{10} fits best if regression is performed on two overlapping groups (Callaghan et al. 2008b, Fig. 1). The first group includes all wind speed measurements below 11.25 m s^{-1}, and cubing and rearranging $W^{1/3} = a'U_{10} + b'$ results in $W = 3.18 \times 10^{-3}(U_{10} - 3.70)^{3}$. A threshold of 3.70 m s^{-1} agreed well with the finding of Monahan and O'Muircheartaigh (1986) that whitecapping is only negligible when the wind speed is less than 3 or 4 m s^{-1}. For the second group, all measurements at wind speeds above 9.25 m s^{-1}, $W = 4.82 \times 10^{-4}(U_{10} + 1.98)^{3}$ is found (Callaghan et al. 2008b). Callaghan et al. (2008b) retrieved a wind history trend for the second group, with a significantly higher offset for decreasing winds than for increasing wind speeds.

b. Wind speed and sea state

1) Classification of sea state according to wave development

We can classify sea state by its degree of development. In young developing seas, significant wave heights are growing toward a fully developed height. This mature stage is usually reached when the phase velocity C_p corresponding with the dominant peak wave slightly exceeds the wind speed. When waves reach a mature stage in gusty wind conditions, they keep growing, although at a progressively reduced rate (Cavaleri et al. 2007). Developed waves are usually encountered where the wind has blown steadily for a lengthy period or where "swell" from an earlier period of stronger winds is present. Increased wave breaking and hence higher levels of W was expected for developed seas. The term C_p can be calculated using $C_p = gT/(2\pi)$, where g is the gravitational acceleration (9.8 m s^{-2}) and T is the wave period.

Another approach for classifying developed and developing sea state is by defining significant wave height for fully developed seas. Various authors have proposed definitions. Carter (1982) gives the wave height of fully developed wave H_{fd} as

$$H_{\mathrm{fd}} = 0.02466U_{10}^{2}, \tag{3}$$

whereas according to Chen et al. (2002) the fully developed wave height is calculated differently for low and high wind speeds,

$$H_{\mathrm{fd}} = 1.614 \times 10^{-2} U_{10}^2 \quad \text{for} \quad 0 \le U_{10} \le 7.5 \qquad (4)$$

and

$$H_{\mathrm{fd}} = 10^{-2} U_{10}^2 + 8.314 \times 10^{-4} U_{10}^3 \quad \text{for} \quad 7.5 \le U_{10} \le 50. \qquad (5)$$

2) Classification of sea state in wind and swell waves

Sugihara et al. (2007) took whitecap images from an oceanographic tower, located 2 km from the coast. Wind speed at 10-m height, varying between 4.64 and 16.57 m s^{-1}, and significant wave height, ranging between 0.27 and 2.92 m, were considerably lower than during the MAP survey. Sea state and wind data were classified as pure windsea (p), counter swell (c), following swell (f), and cross swell (x). Evaluation reveals that whitecaps are mainly ruled by wind waves, and that whitecapping is suppressed by the presence of swell. This is recognized in the offset being larger for p data points than for c, f, and x combined (Sugihara et al. 2007, Fig. 12). At another coastal site, Callaghan et al. (2008a) found that W values were relatively smaller in swell-dominated seas than in mixed seas.

3) Breaking wave parameter R_B

Zhao and Toba (2001) analyzed a range of whitecap datasets obtained in a wind-wave tunnel, at an oceanographic tower and during field surveys, and concluded the breaking wave parameter R_B is the best parameter available to use in parameterization of the wave-breaking process. The term R_B may be interpreted as a type of Reynolds number (Zhao and Toba 2001). They find using least squares regression

$$W = 3.88 \times 10^{-5} R_B^{1.09} \qquad (6)$$

($R^2 = 0.77$), with dimensionless parameter R_B defined by

$$R_B = u_*^2 / \nu_a \varpi_p, \qquad (7)$$

where ν_a is the kinematic viscosity of air, ω_p is the peak angular velocity of wind waves, and u_* is the friction velocity derived from wind speed and drag coefficient C_d at 10-m height using

$$u_* = C_d^{1/2} U_{10}. \qquad (8)$$

Earlier, Wu (1979) used Eq. (8), along with the idea that whitecap coverage is proportional to the rate at which work is being done on the sea surface by wind (i.e., to the product of wind stress and surface drift velocity) to conclude that $W = \alpha u_*^3 = \alpha C_d^{3/2} U_{10}^3$.

4) Reynolds number R_H

Zhao and Toba (2001) propose another kind of non-dimensional Reynolds number R_H for wind waves with velocity and length scales represented by u_* and significant wave height H_s, respectively,

$$R_H = u_* H_s / \nu_a. \qquad (9)$$

Linear regression of the log–log relation between R_H and H_s over the extensive datasets they had accessed results in

$$W = 4.02 \times 10^{-5} R_H^{0.96} \qquad (10)$$

($R^2 = 0.71$). As suggested by Zhao and Toba (2001), using the kinematic viscosity of water ν_w instead of the kinematic viscosity of air might be better conceptually. Woolf (2005) reinforced this suggestion, using

$$R_{Hw} = u_* H_s / \nu_w, \qquad (11)$$

with $\nu_w = 1.26 \times 10^{-6}$ m^2 s^{-1}, the value of kinematic viscosity in seawater for temperature ranging between 13° and 13.8°C (Riisgård and Larsen 2007).

5) Wind speed and wave height

Woolf (2005) suggests a theoretical relation between whitecap coverage and the wind speed and significant wave height of the sea based on the simple assumption that energy dissipation of breaking waves ε is proportional to the product of wave height and wind speed, $H \cdot U$. In combination with Eqs. (10) and (11), this leads to the proposition that

$$W \propto R_{Hw}. \qquad (12)$$

6) Energy dissipation of waves

The suggestion that whitecap coverage is proportional to the rate of energy dissipation from the wave field was made by Cardone, as described in Ross and Cardone (1974), and is now widely accepted. Hwang and Sletten (2008) have proposed a specific relationship to wind and sea state based on a specific theory of energy dissipation from the wave field. An estimate of energy dissipation of wind waves ε (W m^{-2}) is

$$\varepsilon = \alpha \rho_a U_{10}^3, \quad \text{with} \quad \alpha = 0.20\, \varpi_*^{3.3} \eta_*. \qquad (13)$$

The air density ρ_a is taken to be 1.20 kg m^{-3}. Wave parameters $\omega_* = \omega_p U_{10}^3 / g$ and $\eta_* = \eta_{\mathrm{rms}}^2 g^2 / U_{10}^4$ are dimensionless reference wave frequency and wave variance, respectively; ω_p is the spectral peak frequency; and

η^2_{rms} is the variance of surface displacement ($\eta_{\text{rms}} = \frac{1}{4} H_s$). Applying Eq. (13) to an extensive dataset of whitecap observations predicts, for fractional W,

$$W = 0.014(\varepsilon - \varepsilon_c), \tag{14}$$

with threshold energy dissipation for whitecap detection ε_c between 0.013 and 0.038 W m^{-2} (Hwang and Sletten 2008, Fig. 6b). The used dataset comprises wind speeds up to about 20 m s^{-1} and calculated ε values ranging from about 0.1 to 5 W m^{-2}.

3. Datasets

a. In situ data obtained during the MAP campaign

In situ data were acquired during the MAP campaign in June 2006 in the northeast Atlantic. The MAP study area, located between 55.5° and 57.5°N latitude and between 13° and 9.5°W longitude, and methodology are detailed in Callaghan et al. (2008b). On days 17, 19, 20, 21, 22, 27, and 28, whitecap images were analyzed to maximize the range of wind speeds encountered during the field campaign. On the order of hundreds of images should be averaged to achieve convergent values of one W data point (Callaghan et al. 2008a; Callaghan and White 2009). This condition was met by analyzing all sea surface images obtained within a 30-min sampling period. Automated Whitecap Extraction (AWE) was applied to all images; AWE automatically determines the optimal threshold intensity for whitecap detection for every individual image (Callaghan et al. 2008a; Callaghan and White 2009). The value of W was subsequently calculated as the percentage of pixels with intensity value above the threshold value. Wind speed was measured 27 m above sea level in meters per second, and the wind profile power law, $U_{10} = U_{27}(10/27)^{1/7}$, was applied to calculate wind speed at 10-m height. The U_{10} values were averaged over the half-hour periods, uncorrected for flow distortion effects caused by the research vessel. The standard error of U_{10} was estimated at ±1 m s^{-1}. A total of 43 158 images were analyzed to produce 107 data points with U_{10} ranging between 4.6 and 23.1 m s^{-1} and W between 0.002% and 7.5%.

b. QuikSCAT satellite wind vector data

QuikSCAT data are from the SeaWinds microwave scatterometer that was launched on the QuikSCAT satellite in June 1999 (information online at http://winds.jpl.nasa.gov/missions/quikscat). The primary mission of the SeaWinds scatterometers is to measure wind speed and direction at 10-m height over the ocean surface. SeaWinds radiates microwave pulses using a rotating dish antenna with two spot beams that sweep in a circular pattern and measures backscattering. The backscattered power relates to the earth's surface roughness; for water surfaces, the surface roughness is highly correlated with near-surface wind speed and direction. The instrument collects data in a continuous, 1800-km-wide band. QuikSCAT data are produced by Remote Sensing Systems, and sponsored by the National Aeronautics and Space Administration (NASA) Ocean Vector Winds Science Team. Data are available online (at http://www.remss.com). We downloaded all wind vector data files for the North Atlantic for the second half of June 2006. There are two measurements per day, relating to a morning and evening pass. For each MAP station, we used the pass that was closest to the station's time. The scatterometer orbital data is mapped to a 0.25° × 0.25° earth grid, and we interpolated the gridded data to the stations' locations using bilinear interpolation.

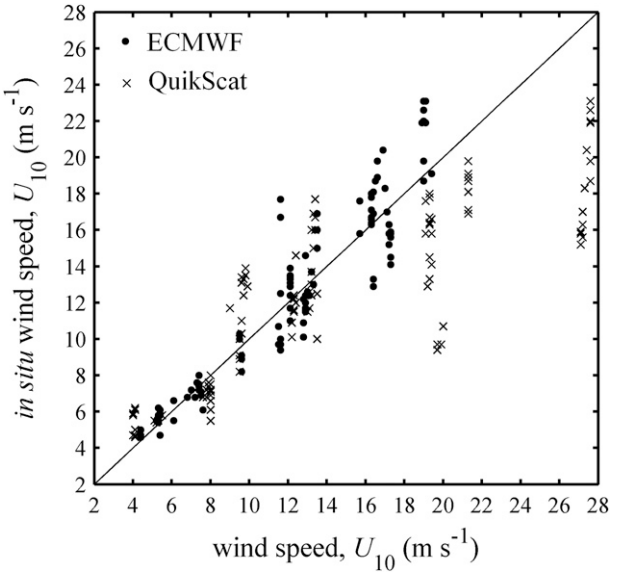

FIG. 1. Scatterplot of in situ U_{10}, obtained during the MAP survey, vs U_{10} derived from ECMWF wave model and QuikSCAT satellite data, with black dots indicating ECMWF and crosses indicating QuikSCAT values. The black line shows a one-to-one relation.

The relation between backscatter coefficient and QuikSCAT wind speed is described by a saturation curve, with decreasing sensitivity for wind speeds over 15 m s^{-1} (Quilfen et al. 2007). This possibly explained QuikSCAT's bigger discrepancy between QuikSCAT and in situ wind speed for higher winds, which appeared to be an overestimation (Fig. 1). The mean absolute error due to the time difference between station and overpass, estimated from a time series at (56.5°N, 11°W), was 1.3 m s^{-1}, whereas the mean absolute error between interpolated wind speed at a station location and its closest 0.25° × 0.25° grid point was 0.4 m s^{-1}. The specification error of SeaWinds is 2 m s^{-1}, resulting in

a total error of $\Delta U_{10} = [(1.3)^2 + (0.4)^2 + (2)^2]^{1/2} = 2.4$ m s^{-1}. This estimation was roughly the same as the root mean square error (RMSE) of 2.5, of a linear least squares fit between QuikSCAT and in situ wind speed.

c. ECMWF data

The ECMWF offers data of global meteorological quantities such as ocean winds and waves. The analysis is produced by ECMWF's Integrated Forecasting System (IFS), a coupled atmosphere–wave model, with assimilation of reliable observational datasets. We obtained a dataset of modeled wind and wave parameters from ECMWF's operational archive for all days of the month of June 2006, consisting of 6-hourly records (at 0000, 0600, 1200, and 1800 UTC), covering the area between 50° and 60°N latitude and between 8° and 15°W longitude on a 0.25° × 0.25° grid. The gridded data were interpolated to the MAP stations' coordinate pairs using bilinear interpolation. For each MAP data point, we selected the ECMWF record that fell within a time span of 3 h of the MAP recording. The following ECMWF parameters were examined: wind speed at 10-m height (WIND), significant wave height (SWH), significant height of wind waves (SHWW), mean wave period (MWP), mean period of wind waves (MPWW), mean direction of wind waves (MDWW), mean direction of total swell (MDTS), and coefficient of drag with waves (CDWW) (http://www.ecmwf.int/publications/manuals/d/gribapi/param).

For strong winds the ECMWF winds were generally lower than the in situ winds (Fig. 1). It is known that the 40-yr ECMWF Re-Analysis (ERA-40), a reanalysis product of ECMWF using an earlier data assimilation system, underestimates high wind speeds (Caires and Sterl 2003, 2005). The absolute wind speed error introduced by the difference between station and ECMWF record time, estimated from a time series at (56.5°N, 11°W), was 0.7 m s^{-1} on average. The uncertainty in WIND was unknown; however, assuming 1 m s^{-1} and a mean absolute error caused by spatial difference of 0.4 m s^{-1} (section 3b), a total error of $\Delta U_{10} = [(0.7)^2 + (0.4)^2 + (1)^2]^{1/2} = 1.3$ m s^{-1} was calculated. The progression of the wind speed error partly explained the RMSE of 1.7, of a linear least squares fit between WIND and in situ wind speed.

d. Data treatment

We used LabFit (Silva and Silva 2010) to perform nonlinear curve fittings over the W data and to derive coefficients $\{a, b, \ldots\}$ and their uncertainties $\{s_a, s_b, \ldots\}$, coefficient of determination R^2; and RMSE. Coefficient a_2 was considered to be significantly different from coefficient a_1 if $|a_2 - a_1| > s_{a1}$. RMSE values were calculated as $\sqrt{1/N - 2\sum(W_i - W)^2}$ (Middleton 2000), where W_i and W are the observed and fitted values of N data points. We used the RMSE as an objective measure of goodness of fit. The propagation of errors in applied parameters such as $\Delta U_{10,}$ as well as unexplained scatter caused by unknown factors, contributes to the RMSE. Curve fitting results are shown in Table 1, and the regression equations are labeled by the letter r, followed by an Arabic number [e.g. Eq. (r3)].

Using nonlinear curve fitting, the error in W on variable x was minimized, instead of minimizing the error in $\log(W)$ on $\log(x)$ for power relations (Zhao and Toba 2001) or the error in $W^{1/3}$ on x for cubed relations (Monahan and Lu 1990; Sugihara et al. 2007; Callaghan et al. 2008b). Because we were comparing various parameterizations, we applied nonlinear curve fitting to all relationships. The regression equations were illustrated in figures similar to how the parameterizations were introduced earlier. Consequently, it may appear to the reader that particular lines do not fit the data displayed in log–log space or on an x–$y^{1/3}$ scale very well.

Analysis of variance (ANOVA) using Matlab function "anova1.m" was applied to compare different groups of W data. It returns the P value for the null hypothesis that the means of the groups are equal.

4. Results

a. Wind speed only

1) Power law

Starting with this "wind speed only" parameterization, we found an exponent of 2.70 using all the in situ data, almost identical to the power-law exponent determined using whitecap data collected in the same region of the North Atlantic (Monahan and O'Muircheartaigh 1986). Eqs. (r1)–(r3) derived using in situ, ECMWF, and QuikSCAT wind speed data differed significantly, with respective exponents 2.7, 3.8, and 1.9, showing that the power relation between W and U_{10} not only depended on location and sea state conditions but also on the wind speed data source. The corresponding RMSE values implied that the error of the fit was smallest for in situ data and increasingly larger for ECMWF and QuikSCAT data.

2) Grouping in low and high wind speeds

Fitting the low and high wind speed whitecap data to Eq. (2) resulted in Eqs. (r4) and (r6). The slopes and intercepts of Eqs. (r4) and (r6) were not significantly different than if $W^{1/3}$ was linearly fitted to U_{10}, and rearranged to conform to Eq. (2) (Callaghan et al. 2008b). If W data were plotted with ECMWF wind speed values, different relations between lower and higher wind speeds were not obvious (Fig. 2a), and fitting all ECMWF wind

TABLE 1. Nonlinear curve fitting results of the various W parameterizations, using in situ U_{10} (3.70–23.09 m s^{-1}) and W (%) values and using ECMWF wave model data to describe sea state. Fits were also calculated using ECMWF and QuikSCAT U_{10} data. Shown are the fitted equation; applied curve; present conditions; applicable wind speed range and source; the a and b curve fitting coefficients and s_a and s_b, their respective uncertainties; the coefficient of determination R^2; the RMSE of the fit; and $\Delta W(U_{10})$, the estimated progression of the error in U_{10} [Eq. (15)].

Eq.	Conditions	Range U_{10}	Source U_{10}	$a \pm s_a$	$b \pm s_b$	R^2	RMSE	$\Delta W(U_{10})$
				Law: aU_{10}^b				
r1	None	Full	In situ	$(15.9 \pm 5.6) \times 10^{-4}$	2.70 ± 0.12	0.90	0.6	0.3
r2	None	Full	ECMWF	$(9.51 \pm 5.6) \times 10^{-5}$	3.76 ± 0.20	0.89	0.7	0.5
r3	None	Full	QuikSCAT	$(11.5 \pm 5.0) \times 10^{-3}$	1.86 ± 0.14	0.80	0.9	0.5
				Law: $a(U_{10} + b)^3$				
r4	None	<11.25	In situ	$(35.7 \pm 9.4) \times 10^{-4}$	-3.83 ± 0.54	0.88	0.15	0.14
r5	None	<11.25	QuikSCAT	$(17.2 \pm 5.0) \times 10^{-3}$	-5.69 ± 0.37	0.75	0.3	
r6	None	>9.25	In situ	$(46.9 \pm 7.3) \times 10^{-5}$	2.28 ± 1.1	0.84	0.7	0.4
r7	None	>9.25	QuikSCAT	$(7.94 \pm 1.9) \times 10^{-5}$	13.5 ± 2.9	0.71	1.0	
r8	None	Full	ECMWF	$(14.4 \pm 2.1) \times 10^{-4}$	-2.89 ± 0.69	0.89	0.7	
r9*	Decreasing wind	>9.25	In situ	5.86×10^{-4}	2.00	0.89		
r10*	Increasing wind	>9.25	In situ	5.66×10^{-4}	0.20	0.92		
r11	Developed	>9.25	In situ	$(41.8 \pm 18) \times 10^{-5}$	3.84 ± 2.6	0.72	0.6	0.4
r12	Developing	>9.25	In situ	$(62.8 \pm 12) \times 10^{-5}$	0.105 ± 1.2	0.88	0.8	0.5
r13	x	>9.25	In situ	$(85.9 \pm 4.3) \times 10^{-6}$	11.7 ± 4.3	0.64	0.2	0.16
r14	p, f	>9.25	In situ	$(34.3 \pm 5.7) \times 10^{-5}$	4.82 ± 1.3	0.83	0.8	0.5
				Law: aR_B^b				
r15	None	Full	In situ	$(28.6 \pm 9.8) \times 10^{-5}$	0.86 ± 0.03	0.94	0.5	0.2
r16	None	Full	ECMWF	$(9.45 \pm 6.0) \times 10^{-5}$	0.96 ± 0.06	0.88	0.7	
r17	None	Full	QuikSCAT	$(18.6 \pm 9.3) \times 10^{-4}$	0.66 ± 0.04	0.85	0.8	
r18	$R_B < 5 \times 10^3$	<8.6	In situ	$(8.28 \pm 9.1) \times 10^{-7}$	1.51 ± 0.14	0.87	0.03	0.03
r19	$R_B < 5 \times 10^3$	<8.6	ECMWF	$(1.07 \pm 1.7) \times 10^{-5}$	1.17 ± 0.20	0.76	0.03	
r20	$R_B < 5 \times 10^3$	<9.3	QuikSCAT	$(43.3 \pm 7.8) \times 10^{-6}$	0.97 ± 0.22	0.69	0.03	
				Law: aR_{Hw}^b				
r21	None	Full	In situ	$(4.51 \pm 2.9) \times 10^{-6}$	0.91 ± 0.04	0.92	0.6	0.1
r22	None	Full	ECMWF	$(4.70 \pm 4.3) \times 10^{-6}$	0.91 ± 0.06	0.86	0.7	
r23	None	Full	QuikSCAT	$(3.14 \pm 2.4) \times 10^{-5}$	0.77 ± 0.05	0.87	0.8	
r24	$R_{Hw} < 2.5 \times 10^5$	<8.7	In situ	$(1.53 \pm 3.6) \times 10^{-8}$	1.34 ± 0.20	0.82	0.02	0.00
r25	$R_{Hw} < 2.5 \times 10^5$	<8.6	ECMWF	$(1.22 \pm 2.8) \times 10^{-7}$	1.16 ± 0.20	0.76	0.03	
r26	$R_{Hw} < 2.5 \times 10^5$	<8.6	QuikSCAT	$(3.93 \pm 9.6) \times 10^{-7}$	1.05 ± 0.21	0.73	0.03	
				Law: $aR_{Hw} \propto H_S$				
r27	Using SWH	Full	In situ	$(10.2 \pm 0.22) \times 10^{-7}$		0.91	0.6	0.1
r28	Using SWH	Full	ECMWF	$(10.4 \pm 0.31) \times 10^{-7}$		0.84	0.8	
r29	Using SWH	Full	QuikSCAT	$(7.63 \pm 0.23) \times 10^{-7}$		0.83	0.8	
r30	Using SHWW	Full	In situ	$(11.3 \pm 0.23) \times 10^{-7}$		0.92	0.6	0.1
r31	Using SHWW	Full	ECMWF	$(11.7 \pm 0.32) \times 10^{-7}$		0.86	0.8	
r32	Using SHWW	Full	QuikSCAT	$(8.47 \pm 0.25) \times 10^{-7}$		0.85	0.8	
				Law: $a(\varepsilon + b)$				
r33	None	Full	In situ	0.882 ± 0.02	0.184 ± 0.08	0.93	0.5	0.3
r34	None	Full	ECMWF	1.05 ± 0.04	0.002 ± 0.09	0.88	0.7	
r35	None	Full	QuikSCAT	0.420 ± 0.02	1.22 ± 0.31	0.81	0.9	
r36	$\varepsilon < 0.2$	<8.3	In situ	0.973 ± 0.09	0.004 ± 0.01	0.80	0.02	0.01
r37	$\varepsilon < 0.2$	<8.7	ECMWF	0.865 ± 0.10	0.004 ± 0.01	0.75	0.03	
r38	$\varepsilon < 0.2$	<8.2	QuikSCAT	0.632 ± 0.09	0.022 ± 0.02	0.68	0.03	

* Relation taken from Callaghan et al. (2008b).

speed data resulted in Eq. (r8). Using QuikSCAT wind speed values, the segregation in the W data points did appear, similarly to the in situ observations (Fig. 2b). Fitting the data to Eq. (2) over lower and higher wind speeds gave Eqs. (r5) and (r7), respectively. The outliers located around $U_{10} = 20$ m s^{-1} and $W < 1\%$ coincided with an up to 7-h time difference between station and QuikSCAT overpass time. In agreement with Callaghan et al. (2008b), binning the W data points in 1 m s^{-1} intervals of ECMWF and QuikSCAT wind speed resulted in approximately identical equations as using the unbinned data.

3) EFFECT OF WIND HISTORY

The wind history trend retrieved by Callaghan et al. (2008b) for high wind speed in situ data [Eqs. (r9) and (r10)] was examined using ECMWF and QuikSCAT

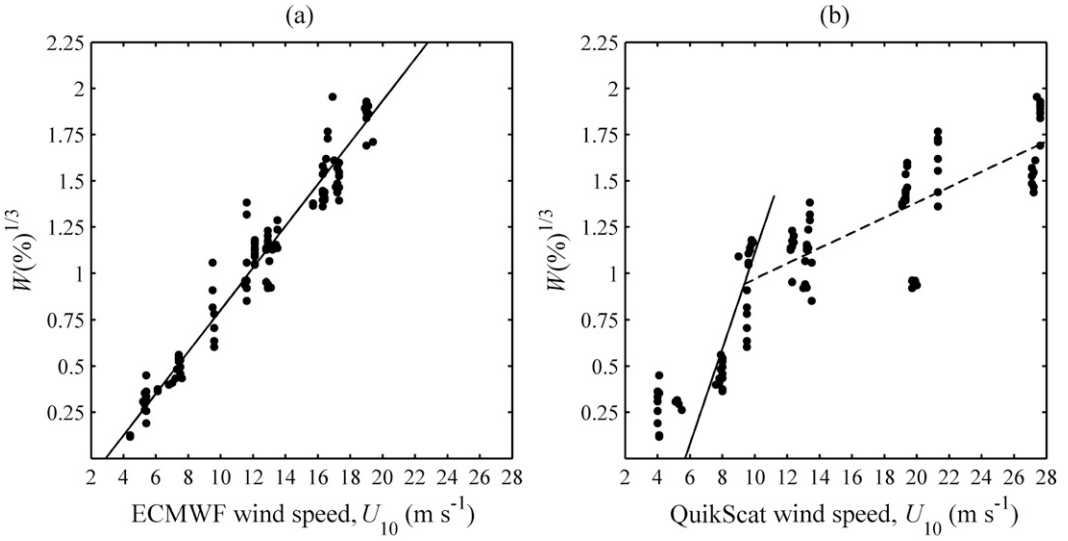

FIG. 2. Scatterplots of $W^{1/3}$ against U_{10}. The W data were acquired during the MAP survey, whereas corresponding U_{10} values at the stations were derived from (a) ECMWF data [solid line represents Eq. (r8)] and (b) QuikSCAT satellite wind vectors [solid and dashed lines represent Eqs. (r5) and (r7), respectively].

wind speed data. ECMWF wind speed was defined to be increasing if the previous 6-hourly wind speed value was lower, decreasing if this value was higher and unchanged if it was the same. The equivalent was done for QuikSCAT wind speed by examining the previous overpass. A scatterplot of the ECMWF data (Fig. 3a) did not show any apparent grouping in terms of wind history, whereas for the QuikSCAT data (Fig. 3b) the case for grouping was ambiguous. ANOVA was applied to test if W data points from increasing and decreasing wind histories were significantly different for wind speeds over 9 m s^{-1}. To remove wind speed dependence from QuikSCAT data, fit residuals between W and Eq. (r7) were calculated. Unlike Callaghan et al. (2008b), the ANOVA showed that the difference between the two cases was not statistically significant. In summary, we could not verify a wind history dependence using either the QuikSCAT or the ECMWF wind speed data.

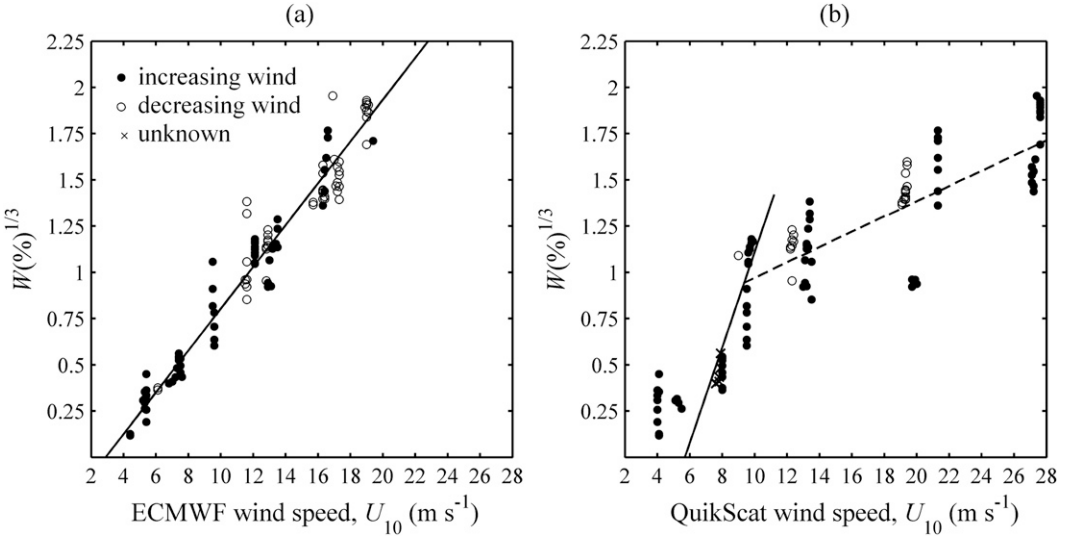

FIG. 3. Scatterplots of $W^{1/3}$ against U_{10}, with black dots indicating data points from periods of increasing wind, open circles indicating data points from periods of decreasing wind, and crosses indicating data points from unchanging wind. The W data were acquired during the MAP survey, whereas corresponding U_{10} values were derived from (a) ECMWF data, with wind history derived from the previous 6-hourly synoptic time, and (b) QuikSCAT satellite wind vectors, with wind history derived from the previous overpass. Solid and dashed lines are as in Fig. 2.

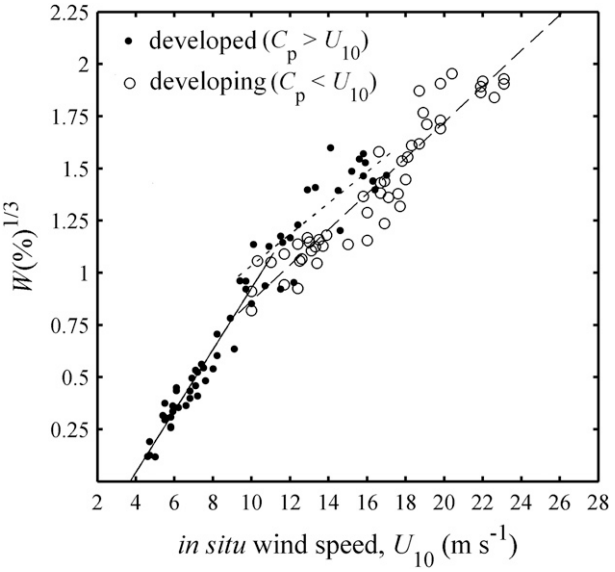

FIG. 4. Scatterplot of $W^{1/3}$ against U_{10}, with black dots indicating developed sea and open circles indicating developing sea. The W and U_{10} data were acquired during the MAP survey. Classification was achieved calculating phase speed C_p from ECMWF's values for mean wave period. Solid, dotted, and dashed lines represent Eqs. (r4), (r11), and (r12), respectively.

b. Wind speed and sea state

1) CLASSIFICATION OF SEA STATE ACCORDING TO WAVE DEVELOPMENT

The in situ data were grouped into developed ($C_p > U_{10}$) and developing ($C_p < U_{10}$) sea states, with C_p estimated using MWP (Fig. 4). Using in situ wind speeds, the wave field was developed for wind speeds below 9.7 m s^{-1}, whereas for wind speed levels over 18 m s^{-1} all waves were developing. Between wind speeds of 9.7 and 18 m s^{-1}, both developed and developing waves occurred, with W values generally higher for the developed sea state than for the developing sea state. This was illustrated by a significantly higher offset in the respective cubed relations between U_{10} and W [Eqs. (r11) and (r12)]. ANOVA revealed a P value of 0.006 for the residuals between Eq. (r6) and developed and developing W data points. If we considered the ECMWF or QuikSCAT wind speed values, instead of the in situ values, no clear difference between developed and developing sea states could be detected (Fig. 5).

SWH values were also used in combination with in situ wind speed to separate developed and developing wave conditions. SWH during the MAP survey varied between 1.0 and 7.8 m, with a mean value of 3.8 m. Applying either Carter's (1982) or Chen et al.'s (2002) equations, shown in Figs. 6a,b, resulted in similar relations between U_{10} and W as when the data were separated according to the phase speed of the waves [Eqs. (r11) and (r12)].

2) CLASSIFICATION OF SEA STATE IN WIND AND SWELL WAVES

We classified the MAP whitecap data with the help of wave data from the ECMWF dataset. If the ratio SHWW/SWH was larger (smaller) than 0.9, the sea state

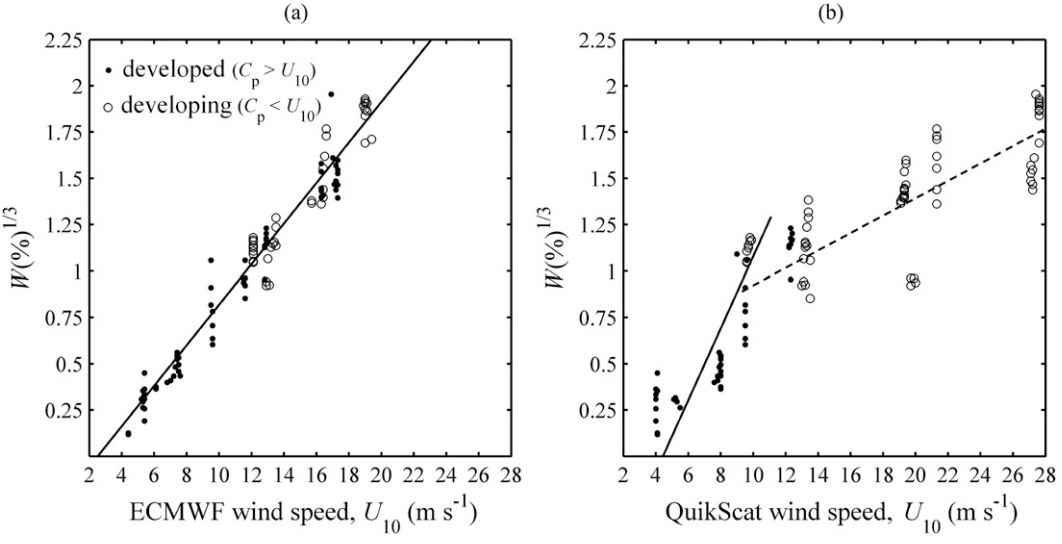

FIG. 5. Scatterplots of $W^{1/3}$ against U_{10}, with black dots and open circles as in Fig. 4. Classification was achieved calculating phase speed C_p from ECMWF's values for mean wave period. The W data were acquired during the MAP survey, and the U_{10} data were derived from (a) ECMWF data and (b) QuikSCAT wind vectors. Solid and dashed lines are as in Fig. 2.

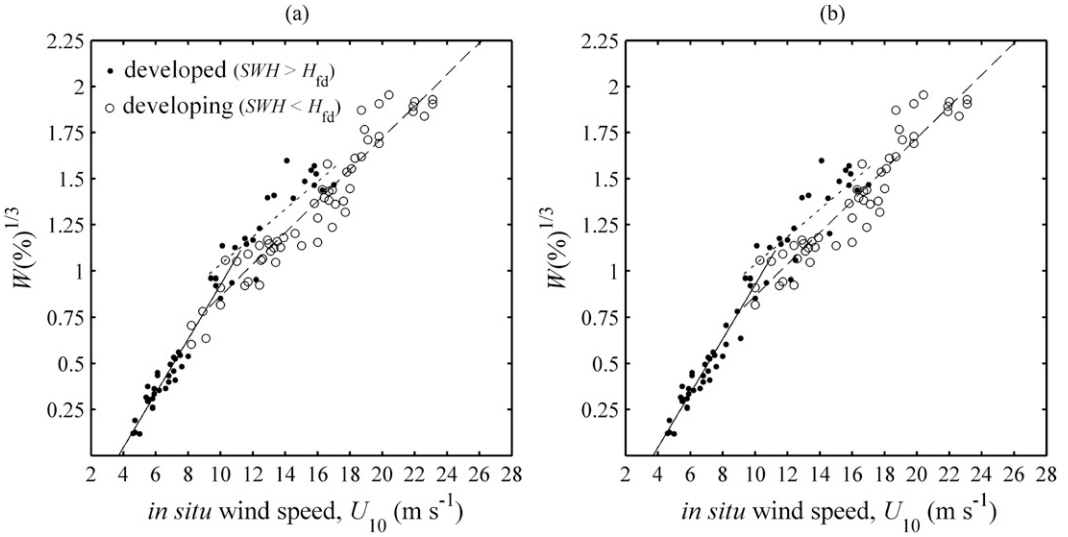

FIG. 6. Scatterplot of $W^{1/3}$ against U_{10}, with black dots and open circles as in Fig. 4. The W and U_{10} data were acquired during the MAP survey. Classification was achieved by comparing SWH, with fully developed wave height H_{fd} calculated using (a) Eq. (3) (Carter 1982) and (b) Eqs. (4) and (5) (Chen et al. 2002). Solid, dotted, and dashed lines are as in Fig. 4.

was classified as pure windsea (mixed sea). Like Sugihara et al. (2007), mixed seas were classified as following swell if the angle between the direction of wind and swell waves was within ±45° and as cross swell if the deflection angle was between ±45° and ±135°. Our dataset did not provide any counter swell conditions (i.e., deflection angles above ±135°). Grouping the W data points in p, f, and x revealed a direct and an indirect dependence on sea state. The indirect dependence was through wind speed (as W increases with wind speed). It can be seen in a scatterplot of the in situ data (Fig. 7) that pure windsea conditions were present for $U_{10} > 12.9$ m s^{-1}, whereas following swell and cross-swell conditions occurred during wind speed ranges 6.8 m s^{-1} < U_{10} < 23.1 m s^{-1} and 4.6 m s^{-1} < U_{10} < 16.9 m s^{-1}, respectively. For the ECMWF and QuikSCAT wind speed data, similar indirect relations existed (Fig. 8). A direct dependence of W on sea state was derived for wind speed values over 9.25 m s^{-1}. Using in situ wind speed (Fig. 7), W was generally smaller during cross swell than during pure windsea and following swell at similar wind speed. Sea state conditions of pure windsea and following swell did not appear to separate the W data points. ANOVA verified a significant difference ($P = 0.002$) between x data and p and f data grouped together. Fitting in situ U_{10} and W data to Eq. (2) gave corresponding Eqs. (r13) and (r14), with significantly different curve fitting coefficients. Using ECMWF or QuikSCAT wind speed values, evidence for dampening of whitecapping during a cross swell was not found (Fig. 8).

3) BREAKING WAVE PARAMETER R_B

We used Eq. (7) with $\nu_a = 0.14 \times 10^{-4}$ m^2 s^{-1} to calculate R_B (Jones and Toba 2001), MPWW to calculate ω_p (with $\omega_p = 2\pi$/MPWW), and CDWW to calculate u_*

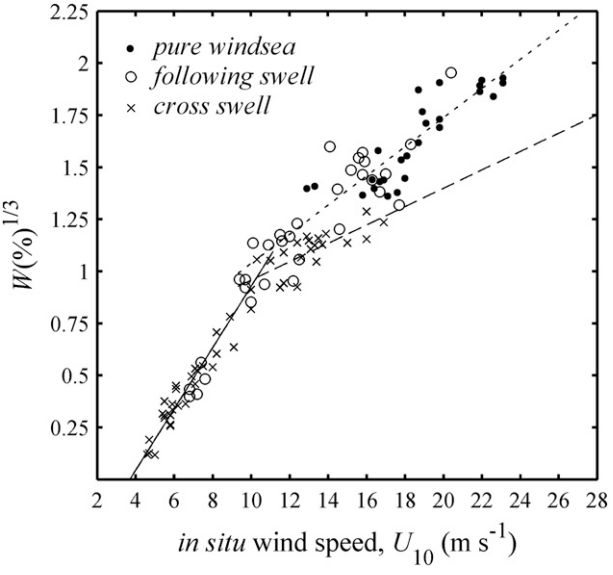

FIG. 7. Scatterplots of $W^{1/3}$ against U_{10}, with black dots indicating W data points during pure windsea (p), open circles indicating W data points during following swell (f), and crosses indicating W data points during cross swell (x). The U_{10} and W data were acquired during the MAP survey, whereas classification (p, f, x) was achieved using ECMWF wave parameters. Solid, dashed, and dotted lines represent Eqs. (r4), (r13), and (r14), respectively.

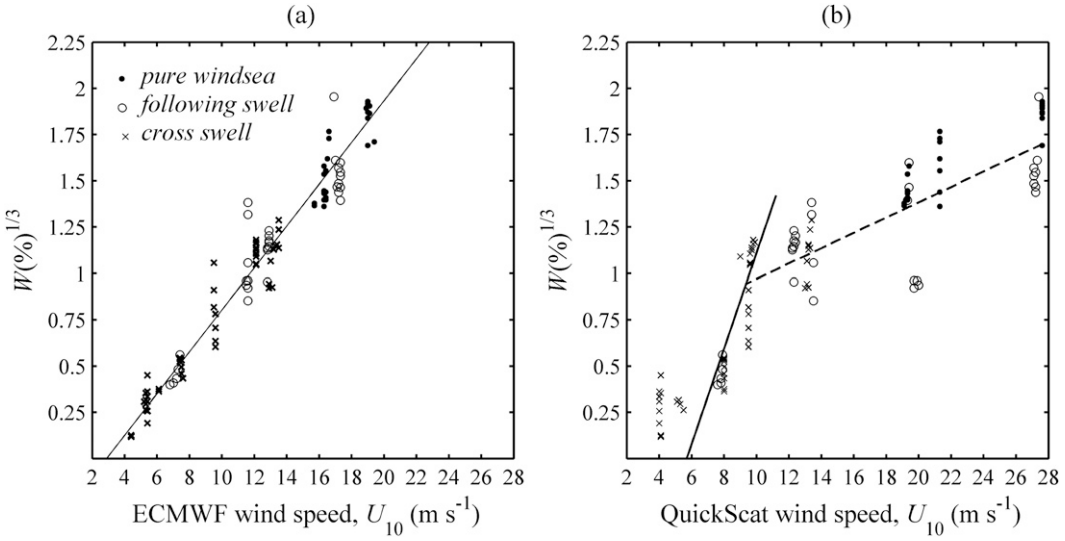

FIG. 8. Scatterplots of $W^{1/3}$ against U_{10}, with black dots, open circles, and crosses as in Fig. 7. Classification (p, f, x) was achieved using ECMWF wave parameters, W data were acquired during the MAP survey, and corresponding U_{10} values were derived from (a) ECMWF data and (b) QuikSCAT wind vectors. Solid and dashed lines are as in Fig. 2.

[Eq. (8)]. Fitting whitecap data points to $W = aR_B^b$, with u_* estimated from in situ U_{10}, resulted in Eq. (r15). Applying ECMWF and QuikSCAT U_{10} data instead produced Eqs. (r16) and (r17), respectively. Here, R_B correlated slightly better with W than the wind speed does, if in situ and satellite measurements of wind speed were considered [(Eqs. (r1) and (r3)]. Using these observational data, knowledge of the sea state (i.e., wave period and drag coefficient) appeared to improve W estimations. No improvement was detected for ECMWF wind speed values [Eqs. (r2) and (r16)].

A scatterplot of W as a function of R_B showed that the W calculations for lower R_B values deviated from the fit (Fig. 9), and there appeared to be a change in slope near $R_B \sim 5 \times 10^3$. The R_B values smaller than 5×10^3 corresponded with wind speed levels below 8.6 m s^{-1} according to in situ and ECMWF data and below 9.3 m s^{-1} according to QuikSCAT data. Fitting the W data over the range $R_B < 5 \times 10^3$ gave Eqs. (r18)–(r20). These fits showed different curve fitting coefficients (i.e., larger slopes and smaller intercepts) than the fits over the full range of R_B values. These differences were significant, except for the slope using U_{10} data from ECMWF [Eqs. (r16) and (r19)].

4) REYNOLDS NUMBER R_H

The value of H_s was estimated using SHWW (SHWW ranged from 0.2 to 7.6 m and was 3 m on average) for the calculation of R_{Hw} [Eq. (11)]. Fitting of the whitecap data to $W = aR_{Hw}^b$, with u_* calculated from in situ, ECMWF, and QuikSCAT wind speed data [Eq. (8)], produced respective Eqs. (r21)–(r23). The relations between R_{Hw} and W for in situ and ECMWF wind speed values were similar and close to Eq. (10). They did not provide better W estimations than the wind speed only relation Eqs. (r1) and (r2).

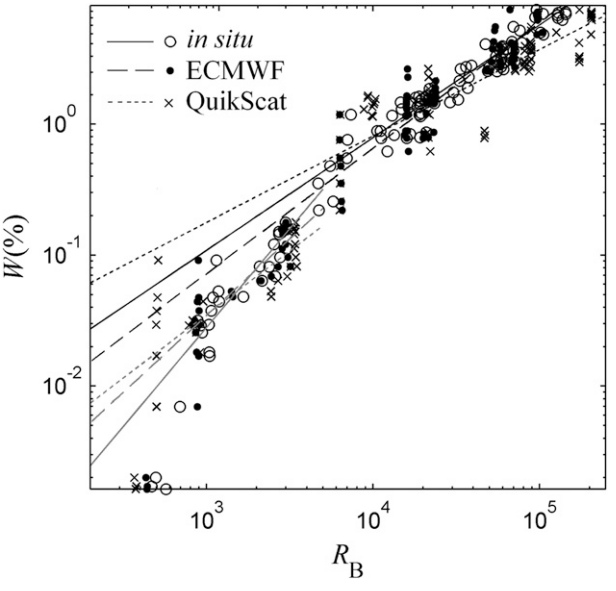

FIG. 9. Scatterplots of W against breaking wave parameter R_B [Eq. (7)], with open circles indicating values calculated using in situ U_{10}, black dots indicating values calculated using U_{10} from ECMWF, and crosses indicating values calculated using U_{10} from QuikSCAT. Black solid, dashed, and dotted lines represent Eqs. (r15)–(r17), respectively, and gray solid, dashed, and dotted lines represent Eqs. (r18)–(r20), respectively.

If we applied the QuikSCAT observations of wind speed, however, the RMSE in W calculations was reduced compared to the wind speed only algorithm Eq. (r3).

Figure 10 shows how W varied with R_{Hw} and a change in relation over lower values could be seen. A value of 2.5×10^5 related with in situ wind speed of 8.7 m s^{-1} and with ECMWF and QuikSCAT wind speeds of 8.6 m s^{-1}. Compared to the fits over the full R_{Hw} range, fits over $R_{Hw} < 2.5 \times 10^5$ showed larger slopes and smaller intercepts [Eqs. (r24)–(r26)]. The significance of the difference between the slopes regarding the ECMWF data was ambiguous [Eqs. (r22) and (r25)].

5) Wind speed and wave height

According to Eq. (12), W is proportional to R_{Hw} and therefore to H_s [Eq. (11)]. Fitting our data to $W = aR_{Hw}$, using in situ U_{10} to derive u_* [Eq. (8)] and SWH for H_s to calculate R_{Hw}, gave Eq. (r27); using ECMWF and QuikSCAT instead of in situ U_{10} resulted in Eqs. (r28) and (r29). Calculating R_{Hw} with significant height of wind waves, instead of significant wave height, resulted in data points similar to those shown in Fig. 10. The relations regarding wind waves [Eqs. (r30)–(r32)] illustrate that the regression slopes were a little but significantly steeper if significant height of wind waves was used instead of significant wave height.

6) Energy dissipation of waves

For parameterizations in terms of energy dissipation of waves, values of α and ε were estimated for the waves during the MAP stations using Eq. (13), with in situ U_{10} and the ECMWF dataset to approximate ω_p (2π/MWP) and $\eta_{\rm rms}$ (¼ × SWH). The variation of W with ε is shown in Fig. 11. Regression between energy dissipation and whitecap coverage in percentage gave Eq. (r33). The relatively low RMSE was comparable to the RMSE of the fit between breaking wave parameter R_B and W [Eq. (r15)]. Figure 11 also illustrates the results of using ECMWF and QuikSCAT U_{10}, instead of in situ U_{10}, described by Eqs. (r34) and (r35). Using ε to estimate W levels, instead of the wind speed only algorithm Eqs. (r1)–(r3), decreased the RMSE for the in situ wind speed values [Eq. (r33)]. We did not see this improvement if we used wave model or satellite wind speed data, however [Eqs. (r34) and (r35)].

In the ε–W plots (Fig. 11), a discrepancy in the fits was shown for energy dissipation levels below ~0.2 W m^{-2}. A value of $\varepsilon = 0.2$ W m^{-2} corresponded with U_{10} values 8.3, 8.7, and 8.2 m s^{-2} from the in situ, ECMWF, and QuikSCAT datasets, respectively. Fitting the W data over $\varepsilon < 0.2$ W m^{-2} resulted in Eqs. (r36)–(r38). These fits performed over $\varepsilon < 0.2$ W m^{-2} produced negligible

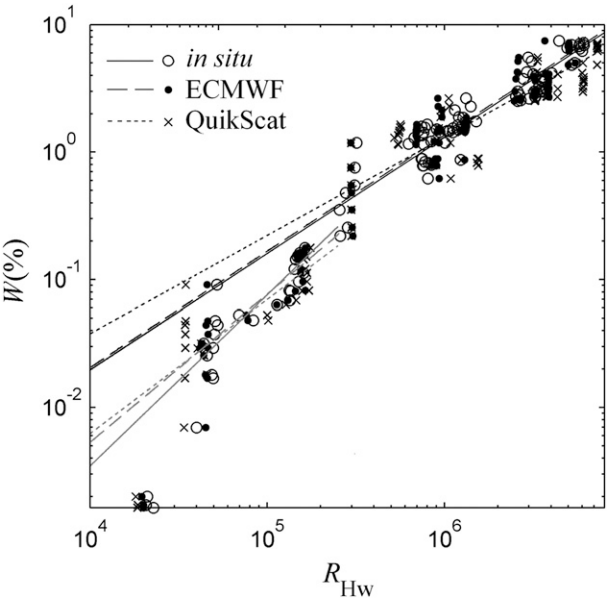

FIG. 10. Scatterplots of W against Reynolds number R_{Hw} for wind waves [Eq. (11)] with open circles, black dots, and crosses as in Fig. 9. Black solid, dashed, and dotted lines represent Eqs. (r21)–(r23), respectively, and gray solid, dashed, and dotted lines represent Eqs. (r24)–(r26), respectively.

intercepts, indicating zero threshold values of energy dissipation. Regarding in situ and QuikSCAT data, the intercepts were significantly smaller and the slopes were steeper than for the fits over all data points. Using ECMWF data, the intercept was similar, whereas the slope was a little smaller.

5. Summary of results and discussion

a. *The grouping of W data in high and low wind speeds*

Analysis of the QuikSCAT wind data confirmed the grouping of W data in low (<11.25 m s^{-1}) and high (>9.25 m s^{-1}) wind speeds. The slope in $W = a(U_{10} + b)^3$ was steeper for low speed values (Fig. 2b), similar to the in situ measurements (Callaghan et al. 2008b). It has to be kept in mind that suspected overestimation of winds over 15 m s^{-1} could have emphasized a gentler slope for higher wind speeds. The ECMWF data did not show any clear division into groups of low and high wind speeds (Fig. 2a). This may be a consequence of the underestimation by the ECMWF of high wind speeds. Here, W was also studied as functions of wave parameters R_B, R_{Hw}, and ε (Figs. 9–11). The revealed changes in the relations around $U_{10} = 8.5$ m s^{-1} (steeper slopes for lower wind speeds) were not unexpected, because all three parameters are a function of U_{10}. The changes were more

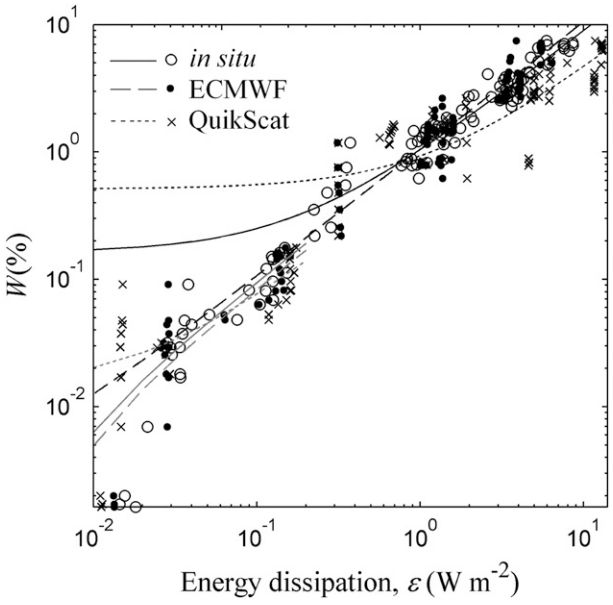

FIG. 11. Scatterplots of W against energy dissipation ε [Eq. (13)] with open circles, black dots, and crosses as in Fig. 9. Wave parameters ω_p and η_{rms} were derived from MWP and SWH. Black solid, dashed, and dotted lines represent Eqs. (r33)–(r35), respectively, and gray solid, dashed, and dotted lines represent Eqs. (r36)–(r38), respectively.

significant if the parameters were calculated with observed U_{10} data (in situ and QuikSCAT) than modeled U_{10} data (ECMWF).

As suggested by Callaghan et al. (2008b), the study of Monahan et al. (1983) offers a physical explanation for the grouping of W data in low and high wind speeds. When wind speed exceeds 10 m s^{-1}, supplementary spume droplets are being formed via the mechanical disruption of wave crests. These droplets are larger and heavier than the spray droplets produced by bursting bubbles, and their interaction with the marine atmospheric boundary layer is different. Spume droplets torn off from breaking crests and sprayed inside the airflow reduce surface drag (Kudryavtsev 2006). According to Andreas (2004), heavier spray droplets slow down near-surface wind by extracting momentum from the wind, and when the spume droplets eventually fall back onto the surface they suppress the shorter waves. Although these effects are thought to only become remarkable at $U_{10} > 20$ m s^{-1} (Andreas 2004; Kudryavtsev 2006), they would agree with a dampening of W, and it may be that described spume droplets effects occur at much lower wind speeds. Another explanation could be that for higher wind speeds underdeveloped waves start occurring (Figs. 4, 6). This would result in less wave breaking and hence less whitecaps than if all waves were fully developed as was seen for lower wind speeds.

b. Effect of wind history and sea state development

Regarding wind speeds over 9.25 m s^{-1}, Callaghan et al. (2008b) found using the in situ MAP data a higher offset in the cubed U_{10}–W relationship for decreasing winds and suggested this was related to degree of wave development. Evidence for a wind history trend using the ECMWF or QuikSCAT wind speed data was not found. However, if ECMWF wave model parameters were used to classify the MAP data in developed and developing wave environments, a larger offset for developed waves was derived [Eqs. (r11) and (r12)]. Because developed waves can be associated with decreasing wind and developing waves can be associated with increasing wind, our finding supported the wind history trend. The observation that W increased with developing stage of the sea is in agreement with the discovery that W increases with wave age (Sugihara et al. 2007).

c. Effect of swell and swell direction

Regarding classification in wave field conditions, W was generally smaller for cross swell, than for following swell and pure windsea conditions combined (Fig. 7). Sugihara et al. (2007) and Callaghan et al. (2008a) both found that the presence of swell dampens whitecapping but did not identify a clear relation with deflection angle between wind and swell waves. A possible reason for reduced whitecapping in the presence of swell may be wave-driven winds, because these winds consume swell energy (Semedo et al. 2009).

d. Evaluation of existing parameterizations

A number of known W parameterizations were evaluated using the MAP dataset by comparing the RMSE values of their fits (Fig. 12). For a simple power relation between in situ U_{10} and W, the RMSE of the fit was 0.6 [Eq. (r1)]. Only a fraction of the scatter in the W data could be explained by the ± 1 m s^{-1} standard error of U_{10}, as clarified in the following. An approximation of the propagation of this error in the calculation of W was derived from

$$\Delta W(U_{10}) = (dW/dU_{10})\Delta U_{10}. \tag{15}$$

Applying Eq. (15) to Eq. (r1), $\Delta W(U_{10}) = 2.70 \times 15.9 \times 10^{-4} \times U_{10}^{1.70}\Delta U_{10}$; using the average value of U_{10} over all stations, 12.6 m s^{-1}, and $\Delta U_{10} = 1$ m s^{-1}, leads to $\Delta W(U_{10}) \approx 0.3\%$. An error of 0.3% would account for less than half of the RMSE in $W(\Delta W_{1+2}^2 = \Delta W_1^2 + \Delta W_2^2)$. The remaining fraction of about 0.5% could be attributed to other factors, and it was assumed that including sea state parameters would reduce this unexplained error in W. The values of the sea state parameters were taken

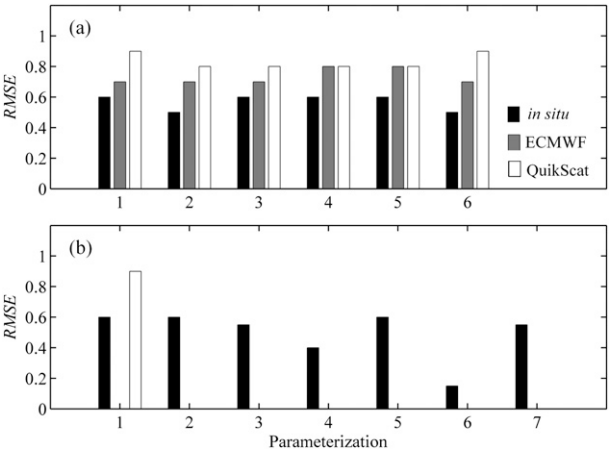

FIG. 12. Bar diagrams showing RMSE values (a) of the nonlinear curve fits of the various W parameterizations using 1) wind speed only [Eqs. (r1)–(r3)]; 2) R_B [Eqs. (r15)–(r17)]; 3) R_H, power relation [Eqs. (r21)–(r23)]; 4) R_H, linear relation [Eqs. (r27)–(r29)]; 5) R_H, linear relation, wind waves [Eqs. (r30)–(r32)]; and 6) ε [Eqs. (r33)–(r35)] and (b) applying a grouping in low (<9.25 m s^{-1}) and high (>9.25 m s^{-1}) U_{10} and for the high U_{10} using 1) no conditions [Eqs. (r4)–(r7)]; 2) grouping according to developing sea state [Eqs. (r4), (r11), and (r12)]; 3) grouping according to the composition of wind and swell waves [Eqs. (r4), (r13), and (r14)]; 4) only developed waves [Eqs. (r4) and (r11)]; 5) only developing waves [Eqs. (r4) and (r12)]; 6) only cross swells [Eqs. (r4) and (r13)]; and 7) only seas that are a combination of pure windsea and following swell [Eqs. (r4) and (r14)].

from or calculated with the ECMWF wave model dataset. A summary of all evaluated parameterizations using MAP data is given in Table 1. The progression of the standard error in U_{10} for lower wind speeds was estimated using $\Delta U_{10} = 0.3$ m s^{-1}, because the standard deviation for wind speeds lower than 9 m s^{-1} was almost 3 times smaller than for wind speeds above (Callaghan et al. 2008b). For higher wind speeds, ΔU_{10} was assumed to be equal to one. By doing so, the approximated standard errors for the grouped wind speeds were on the low side, and the calculated errors indicated the values we could at least expect. Reducing ΔU_{10} by reducing the averaging time was not an option, because U_{10} was averaged over the half-hour periods during which video recordings were taken. Shorter periods would not give the hundreds of whitecap images needed to derive accurate W values. For all groups, the RMSE of the fit was at least double $\Delta W(U_{10})$ (Table 1), leaving room for improvement. An exception was the low wind speed range, for which the RMSE of the wind speed only fit Eq. (r4) was approximately equal to $\Delta W(U_{10})$, indicating that for the MAP data not much could be gained by incorporating additional factors. It is therefore most effective to focus on parameterizations that describe W during high wind speeds. For the independent datasets, a progression of the wind speed error $\Delta W(U_{10}) \approx 0.5\%$ was calculated, applying Eq. (15) to Eqs. (r2) and (r3) and using $\Delta U_{10} = 1.3$ and 2.4 m s^{-1} for the ECMWF and QuikSCAT wind speed data, respectively (sections 3b and 3c). This, $\Delta W(U_{10})$ being approximately equal to the scatter, clarified why efforts to classify W data according sea state conditions were not successful for the independent datasets.

Zhao and Toba (2001) analyzed various datasets by regressing W values against wave age, wave period, U_{10}, friction velocity u_*, breaking wave parameter R_B, and Reynolds number R_H and concluded that R_B has the strongest relation with W. We found for the in situ data that using R_B or energy dissipation of breaking waves ε (Hwang and Sletten 2008) reduced the RMSE in W by 0.1 (Fig. 12a). Using ECMWF wind speed values to calculate R_B or ε did not lead to improved W estimations, and R_{Hw} gave even poorer results (Fig 12a). For QuikSCAT wind speed data, however, an improvement from 0.9 to 0.8 was achieved by using R_B or R_{Hw} (Fig 12a). Applying the classification of W data in lower and higher wind speeds to the full range of in situ and QuikSCAT wind speed data did not advance the wind speed only algorithm (Figs. 12a,b, parameterization 1). High in situ wind speed data could be separated according to developing state or composition of wind and swell waves, but this did not lead to a significant improvement (Fig. 12b, parameterizations 2 and 3). However, if during high wind all waves were developed or all waves were cross swells, the RMSE was expected to reduce significantly, especially for the latter (Fig. 12b, parameterizations 4 and 6).

In summary, we have demonstrated that wind history and wave development are significant to whitecapping, but we have not been able to notably reduce the W data scatter of the MAP dataset by taking sea state parameters into account (Fig. 12). The error in W remained largely unexplained. A range of factors can be thought of.

First, there are possible systematic errors in the ship-based wind speed measurements. The moving vessel probably interfered with the measured airflow, adding a bias or increasing uncertainty in measured wind speed values. Using a logarithmic wind profile law to extrapolate wind speed values at a height of 27 m to 10 m, possible variations in the atmospheric stability were ignored, because not all relevant parameters were measured because of technical difficulties encountered during the cruise (Callaghan et al. 2008b). Other unaccounted effects that could have altered the wind speed profiles were wave-driven winds (Semedo et al. 2009) and slowing of the wind by spume droplets (Andreas 2004). Additionally the half-hour-averaged wind speed measurements did not take

wind speed fluctuations into account. Wind gustiness could have a considerable effect on whitecapping, because mature waves keep growing in gusty winds conditions well above the limit of a fully developed sea obtained in steady wind conditions (Cavaleri et al. 2007). In very unstable conditions, the gain in wave height, denoted by $\Delta H_s/H_s$, may reach values as large as 0.3 (Cavaleri et al. 2007).

Second, many factors in the complex process of whitecapping were absent in the evaluated W parameterizations. Developed seas, indicating bigger waves, were associated with increased whitecapping (Figs. 5, 6) on one hand, but on the other hand swells could also dampen whitecapping (Fig. 7). These two opposing effects implied that the W parameterizations we assessed in this paper were too simple. There are various feedback mechanisms between the sea surface and the atmosphere: for example, the wave-driven winds and spume droplet formation. Wave–wave interaction plays a role in swell dissipation as well: for instance, longer waves enhance the wave breaking of shorter waves (Cavaleri et al. 2007). Also ignored were the interaction of waves with the vertical structure of the upper layers of the ocean and the concentration of surfactants at the sea surface.

Our study looked at the scatter within the MAP dataset, but if knowledge of W is needed in global estimations, for example to calculate carbon or aerosol fluxes, the relation between wind speed and W has to be identified for different locations and during different seasons. Variables affecting this relation, such as fetch conditions, surface salinity, sea surface temperature, and near-surface atmospheric stability, often phrased in terms of the water–air temperature difference ΔT (e.g., Monahan and Woolf 1989), can be very different than present during the MAP survey. According to Monahan and O'Muircheartaigh (1986), apparent latitudinal variation in the exponent of the U_{10}–W power law is explained by both wind duration and mean seawater temperature changing with latitude. Empirical relations derived from previous studies show that power relations between W and U_{10} diverge widely, with exponents ranging between about 2 and 5. Using one equation for the whole globe could obviously lead to very big errors in the calculation of carbon and aerosol fluxes, especially in the high wind speed range. Further study of the relation between W and U_{10} on a global scale, as well as its seasonal variability, is therefore needed. An alternative approach would be to measure W from satellite directly: for example, using microwave radiometry (Anguelova and Webster 2006).

6. Conclusions

Referring to the two objectives stated in the introduction, the following conclusions were derived:

1) Independent datasets reinforced the whitecap study by Callaghan et al. (2008b) based on in situ measurements. The QuikSCAT satellite wind speed data showed a grouping of W data points in low ($<$11.25 m s^{-1}) and high ($>$9.25 m s^{-1}) winds, whereas the wind history trend was coincident with state of wave development assessed using ECMWF wave model data.
2) Whitecapping was proven to be mainly wind driven. Using in situ and QuikSCAT wind speed values, a minor reduction in the scatter of the W data points of the MAP data could be achieved compared to the ''wind speed only'' algorithm, if wave-breaking parameters were applied (Fig. 12a). Classification of the data in high and low wind speeds and according to sea state did not lead to better W estimations (Fig. 12b).
3) All W parameterizations performed better using in situ wind speeds than ECMWF or QuikSCAT wind speeds (Fig. 12).
4) Of the independent datasets, the ECMWF dataset gave the best goodness of fit (Fig. 12a).
5) Grouping of sea state according to wave development, wind history, or the composition of wind and swell waves was not observed for ECMWF or QuikSCAT. It is thought that uncertainties in the wind speed retrievals were too big, concealing any sea state dependence of whitecapping.
6) Using ECMWF or QuikSCAT data, the wind speed only algorithm derived for the MAP data might not apply to other parts of the globe or during different times of the year.
7) The conclusion that developed waves related to increased whitecapping qualitatively supported the postulates that W increases with wave age (Sugihara et al. 2007) and with wave height (Zhao and Toba 2001; Woolf 2005).
8) Cross-swell conditions reduce whitecapping (counteracting the effect described in the previous conclusion).

Finally, our study might not have resulted in a practically improved parameterization of whitecap coverage and the data scatter remained largely unexplained, but it might open doors to a better understanding of wave-breaking and wind-wave interaction.

Acknowledgments. This research is a contribution of the National Centre for Earth Observation, an NERC Collaborative Centre. In addition, we acknowledge financial support received through the UHI Millennium Institute's ARC Programme, an initiative jointly supported by Highlands and Islands Enterprise, the Scottish Funding Council, and the European Regional Development Fund.

The MAP (Marine Aerosol Production) project was an international collaborative effort headed by Prof. Colin O'Dowd (School of Physics and Centre for Climate and Air Pollution Studies, National University of Ireland, Galway, Ireland) and Prof. Gerrit de Leeuw (Climate Change Unit, Finnish Meteorological Institute, Helsinki, Finland and TNO Built Environment and Geosciences, Utrecht, Netherlands) focused on quantifying the production of primary and secondary marine aerosol formation from natural sources. MAP images were collected by Leo Cohen (TNO Defence and Security, Hague, Netherlands) and Gerrit de Leeuw on board the R/V *Celtic Explorer*.

REFERENCES

Andreas, E. L, 2004: Spray stress revisited. *J. Phys. Oceanogr.,* **34,** 1429–1440.

Anguelova, M. D., and F. Webster, 2006: Whitecap coverage from satellite measurements: A first step toward modeling the variability of oceanic whitecaps. *J. Geophys. Res.,* **111,** C03017, doi:10.1029/2005JC003158.

Asher, W. E., L. M. Karle, B. J. Higgins, P. J. Farley, E. C. Monahan, and I. S. Liefer, 1996: The influence of bubble plumes on air-seawater gas transfer velocities. *J. Geophys. Res.,* **101** (C5), 12 027–12 041.

Caires, S., and A. Sterl, 2003: Validation of ocean wind and wave data using triple collocation. *J. Geophys. Res.,* **108,** 3098, doi:10.1029/2002JC001491.

——, and ——, 2005: 100-year return value estimates for ocean wind speed and significant wave height from the ERA-40 data. *J. Climate,* **18,** 1032–1047.

Callaghan, A. H., and M. White, 2009: Automated processing of sea surface images for the determination of whitecap coverage. *J. Atmos. Oceanic Technol.,* **26,** 384–394.

——, G. B. Deane, and M. D. Stokes, 2008a: Observed physical and environmental causes of scatter in whitecap coverage values in a fetch-limited coastal zone. *J. Geophys. Res.,* **113,** C05022, doi:10.1029/2007JC004453.

——, G. de Leeuw, L. Cohen, and C. D. O'Dowd, 2008b: Relationship of oceanic whitecap coverage to wind speed and wind history. *Geophys. Res. Lett.,* **35,** L23609, doi:10.1029/2008GL036165.

Carter, D. J. T., 1982: Prediction of wave height and period for a constant wind velocity using the JONSWAP results. *Ocean Eng.,* **9,** 17–33.

Cavaleri, L., and Coauthors, 2007: Wave modelling—The state of the art. *Prog. Oceanogr.,* **75,** 603–674.

Chen, G., B. Chapron, and R. Ezraty, 2002: A global view of swell and wind sea climate in the ocean by satellite altimeter and scatterometer. *J. Atmos. Oceanic Technol.,* **19,** 1849–1859.

Gordon, H. R., 1997: Atmospheric correction of ocean color imagery in the Earth Observing System era. *J. Geophys. Res.,* **102** (D14), 17 081–17 106.

Hwang, P. A., and M. A. Sletten, 2008: Energy dissipation of wind-generated waves and whitecap coverage. *J. Geophys. Res.,* **113,** C02012, doi:10.1029/2007JC004277.

Jones, I. S. F., and Y. Toba, 2001: *Wind Stress over the Ocean.* Cambridge University Press, 309 pp.

Kudryavtsev, V. N., 2006: On the effect of sea drops on the atmospheric boundary layer. *J. Geophys. Res.,* **111,** C07020, doi:10.1029/2005JC002970.

Middleton, G. V., 2000: *Data Analysis in the Earth Sciences Using Matlab*. Prentice-Hall, 260 pp.

Monahan, E. C., and I. G. G. O'Muircheartaigh, 1986: Whitecaps and the passive remote sensing of the ocean surface. *Int. J. Remote Sens.,* **7,** 627–642.

——, and D. K. Woolf, 1989: Comments on ''Variations of whitecap coverage with wind stress and water temperature.'' *J. Phys. Oceanogr.,* **19,** 706–709.

——, and M. Lu, 1990: Acoustically relevant bubble assemblages and their dependence on meteorological parameters. *J. Oceanic Eng.,* **15,** 340–349.

——, C. W. Fairall, K. L. Davidson, and P. Jones Boyle, 1983: Observed inter-relations between 10m winds, ocean whitecaps and marine aerosols. *Quart. J. Roy. Meteor. Soc.,* **109,** 379–392.

——, D. E. Spiel, and K. L. Davidson, 1986: A model of marine aerosol generation via whitecaps and wave disruption. *Oceanic Whitecaps, and Their Role in Air-Sea Exchange Processes,* E. C. Monahan and G. MacNiocaill, Eds., Springer, 167–174.

O'Dowd, C. D., and G. de Leeuw, 2007: Marine aerosol production: A review of the current knowledge. *Philos. Trans. Roy. Soc.,* **365A,** 1753–1774.

Quilfen, Y., C. Prigent, B. Chapron, A. A. Mouche, and N. Houti, 2007: The potential of QuikSCAT and WindSat observations for the estimation of sea surface wind vector under severe weather conditions. *J. Geophys. Res.,* **112,** C09023, doi:10.1029/2007JC004163.

Riisgård, H. U., and P. S. Larsen, 2007: Viscosity of seawater controls beat frequency of water-pumping cilia and filtration rate of mussels *Mytilus edulis*. *Mar. Ecol. Prog. Ser.,* **343,** 141–150.

Ross, D. B., and V. Cardone, 1974: Observations of oceanic whitecaps and their relation to remote measurements of surface wind speed. *J. Geophys. Res.,* **79,** 444–452.

Semedo, A., Ø. Saetra, A. Rutgersson, K. K. Kahma, and H. Petterson, 2009: Wave-induced wind in the marine boundary layer. *J. Atmos. Sci.,* **66,** 2256–2271.

Silva, W. P., and C. M. D. P. S. Silva, cited 2010: LAB fit curve fitting software (nonlinear regression and treatment of data program), V 7.2.47 (1999-2010). [Available online at http://www.labfit.net.]

Sugihara, Y. H., T. Tsumori, T. Ohga, H. Yoshioka, and S. Serizava, 2007: Variation of whitecap coverage with wave-field conditions. *J. Mar. Syst.,* **66,** 47–60.

Woolf, D. K., 2005: Parametrization of gas transfer velocities and sea-state-dependent wave breaking. *Tellus,* **57B,** 87–94.

——, and Coauthors, 2007: Modelling of bubble-mediated gas transfer: Fundamental principles and laboratory test. *J. Mar. Syst.,* **66,** 71–91.

Wu, J., 1979: Oceanic whitecaps and sea state. *J. Phys. Oceanogr.,* **9,** 1064–1068.

Zhao, D., and Y. Toba, 2001: Dependence of whitecap coverage on wind and wave properties. *J. Oceanogr.,* **57,** 603–616.